Biochemistry and Biophysics Reports 41 (2025) 101922

Contents lists available at ScienceDirect

Biochemistry and Biophysics Reports

journal homepage: www.elsevier.com/locate/bbrep

Development of a general anti-viral therapeutic using cholestosome technology to exploit inhibition of intracellular viral production

Lawrence Mielnicki [a,b], Julie Hughes [a], Mary Irving [a], Mary McCourt [a,b,*]

[a] Department of Chemistry, Biochemistry and Physics, Niagara University, Lewiston, NY, 14109, USA
[b] Niagara University Biomedical Research Institute, 73 High Street, Buffalo, NY, 14203, USA

A B S T R A C T

The recent events of the worldwide Covid-19 pandemic showed the need for a general anti-viral therapeutic, independent of the specific characteristics of the virus, that targets intracellular mechanisms of viral production to prevent the rapid, overwhelming spread of infection and its devastating consequences. The development of the Cholestosome technology, a drug delivery system made exclusively of cholesteryl esters, is a solution for intracellular targeting of viral replication. It is well known that Zn^{2+} is capable of inhibiting viral replication but the control of intracellular Zn^{2+} concentration is tightly regulated. Cholestosome technology can encapsulate Zn^{2+} and deliver it to cells to inhibit viral replication. The human betacoronavirus OC43 (OC43) model system was used to infect cells and infected cells were treated with Zn^{2+} encapsulated in Cholestosomes as well as appropriate controls. Viral production was measured using CPE as well as PCR methods to determine inhibition of infection. Experimental results indicated a 55 % reduction in viral load for those cells treated with Zn^{2+} encapsulated in cholestosomes versus Zn^{2+} alone.

1. Introduction

Viral load is a key driver in the progression of many viral diseases, from HIV to influenza to coronavirus (CoV), increasing the likelihood of latent/persistent infections and severe complications leading to death [1–3]. Nowhere was this more evident than in the recent global COVID-19 Pandemic that still has the world feeling its effects today. The SARS-CoV-2 virus has symptoms that are like the common cold, including fever, sore throat, cough, muscle and chest pain, etc. The manifestation of the disease can vary from being asymptomatic to severe life-threatening conditions warranting hospitalization and ventilation support [4,5]. Viral load is a key driver in the progression of this viral disease enabling the changes seen in the increasing number of identified SARS-CoV-2 variants [6–8]. Although vaccine development has been improved [9], the development of new or repurposing of existing anti-viral therapeutics is still under development after the relative ineffectiveness of their use against COVID-19 and other targets [10–13].

Most therapeutics target extracellular virus, using agents that target specific virus-host interactions such as host protease inhibition to restrict entry of virus, depleting intracellular nucleotide pools, inhibiting glycosidases or kinases and immune system activation [14–16], or agents broadly acting against either host or viral targets important in infection or replication [10,15,17] Thus, the intracellular fraction of the virus escapes this treatment, increasing the likelihood of treatment-resistant long term and latent infections. Targeting the intracellular virus fraction would result in a more robust therapeutic response and reduce or eliminate long-term consequences of viral disease [14]. Mechanisms involved in many of the above processes depend on the presence of zinc [18–21].

Zinc (Zn^{2+}) is a common nutritional supplement that is formulated as a stand-alone antiviral intervention or as a combination nutraceutical containing other vitamins, minerals, and nutrients [22]. Zn^{2+} has the potential to reduce the risk of viral respiratory tract infections, including SARS-CoV-2, and shorten the duration and severity of illness [22]. In vitro studies have demonstrated that Zn^{2+} can inhibit the enzymatic activity and replication of SARS-CoV RNA polymerase and may inhibit angiotensin-converting enzyme 2 (ACE2) activity [23,24]. Zn^{2+} could modify the host's response as Zn^{2+} reduces the permeability of the cell membrane without penetration into or damage to the cell [25,26]. A deficiency in Zn^{2+} can decrease immunity in humans, increasing risk of infection and a delay in healing [25]. Zn^{2+} is therefore a known inhibitor of viral replication but intracellular movement of Zn^{2+} is tightly regulated [22,25,26]. Enhancement of the intracellular concentration of Zn^{2+} is necessary to maximize its antiviral effects and pro-immune properties.

Intracellular delivery of antiviral therapeutics, including anti-COVID antibodies, repurposed molecules (e.g. remdesivir) and Zn^{2+} would offer new weapons in the battle against infection of SARS-CoV-2 and new

* Corresponding author. Department of Chemistry, Biochemistry and Physics, Niagara University, Lewiston, NY, 14109, USA.
E-mail address: mpm@niagara.edu (M. McCourt).

https://doi.org/10.1016/j.bbrep.2025.101922
Received 30 August 2024; Received in revised form 30 December 2024; Accepted 14 January 2025

emerging coronavirus variants as well as other viral pathogens. The development of new modalities to deliver antiviral therapeutics intracellularly is one of the critical unmet needs in the arsenal to combat acute respiratory virus infection [14,27].

The best known delivery system uses liposomes, the development of which as a drug delivery system has a long history [28–30]. Liposomes are easily made and manufactured, but they have not really seen the success that was promised, having functional limitations due to their instability in biological systems and low load ratios [31–37]. Thus, liposomes have seen limited utility as drug delivery vehicles, highlighting the need for novel systems.

Until recently, the use of cationic lipids has also been of limited utility for general delivery of molecular cargo, with their most successful cargo being immunogens against the targets on SARS-CoV-2. The development of this system also has a long history but still requires more study to develop widespread applicability [9,37].

Our laboratory has developed a patented platform-based drug delivery technology using only neutral lipids (cholesteryl esters), called a Cholestosome. A cholestosome is a novel vesicle that can be used to deliver a wide variety of molecules including antibiotics, immunoglobulins (IgG) and small molecules into a diverse array of cell types [38,39]. It can confer a unique oral bioavailability to peptides and proteins enabling their intracellular delivery [39].

Cholestosomes have been used to make insulin orally bioavailable in mice and rats with AUCs higher than intravenous administration and delivery to all tissues examined, including the brain [40–45]. These studies highlight the systemic delivery afforded by cholestosome encapsulation and the potential use of cholestosomes for oral delivery of therapeutic molecules, especially those that have not normally been amenable to this route of delivery. The demonstrated cholestosome mediated intracellular delivery can also be advantageous for enhancing the delivery of highly regulated molecules such as Zn^{2+}. For the reasons stated above, Cholestosome-Zn^{2+} is thus proposed as a generalized antivirus therapeutic.

This present study describes our efforts at treating virus infection with cholestosome encapsulated Zn^{2+} using OC43, a surrogate for SARS-CoV-2 and respiratory infections in general [46–50]. Cholestosomes were used to encapsulate and deliver Zn^{2+} into target cells infected with the OC43. In all cases, cholestosome encapsulated Zn^{2+} inhibited viral replication to a greater extent than unencapsulated Zn^{2+}, with encapsulated Zn^{2+} treated OC43 infected cells showing up to a 55 % reduction in viral load.

2. Materials and methods

Preparation of Zinc-BSA Cholestosomes: Cholestosomes were formulated as described in Ref. [39]. Briefly, 5 mL of aqueous stock solution (100uM Zn^{2+}, 5 mg/ml BSA) was added to a 15 ml conical tube and equilibrated in a water bath at 55 °C. 80 mg of Cholesteryl Myristate and 75 mg of Cholesteryl Laurate (NU Check Prep; Elysian, MN) were put into a 100 mL round bottom flask (RBF) and solubilized with 5 mL of diethyl ether. The flask with the solubilized esters was then put on a Rotovapor R-3 (Buchi, New Castle, DE) to spin at speed setting 4 for 10 min at 55 °C without vacuum. Low vacuum was then applied for 10 min. The RBF was then removed, pre-equilibrated stock solution was added to the RBF followed by sonication at 55° C for 15 min (90 % power, 37 kHz) in an Elmasonic P Sonicator (Tovatech, Maplewood, NJ). RBF was rotated during sonication every 5 min. The resulting Cholestosomes™ were then filtered through a sterile 40 μm nylon mesh strainer (ThermoFisher Scientific, Waltham, MA) and stored at 4 °C until analysis.

Analysis of Cholestosomes: Microscopic analysis was conducted on the EVOS FL AUTO microscope (ThermoFisher Scientific, Waltham, MA). Dynamic light scattering (DLS) and Zeta Potential analysis of Cholestosomes™ was performed with the Lifesizer 500 (Anton Paar, Hanover, VA). Lipid concentrations were determined using a Shimadzu UFLC system (CTO-20A) paired with UV detection (SPD-20AV) including a data acquisition processing system (LCMS 2020, Shimadzu, Columbia, MD). 50uL of injected reconstituted ester mix were separated isocratically for 12.5-min (flow rate of 1.0 mL/min) on a Phenomenex Kinetex 5 μm XB-C18 100 Å column (150 × 4.6 mm) using mobile phase at a temperature of 35 °C. The formulation was diluted tenfold and gravity filtered through a 0.45 μm syringe filter. The amount of encapsulated Zn^{2+} was calculated using a model which is based on vesicle size, the amount of lipid and the starting concentration of the Zn^{2+} [41,42].

Cells and Treatments: Vero, MCF-7, Jurkat, ARPE-19, A549 and HCT8 cells were maintained under standard conditions [46,48,50–54]. For treatments, cells were seeded into 6-well or 24 -well dishes at 2e+4 cells/cm^2, grown until 90 % confluence after which media was replaced with infection media (complete media at 2%FBS). Virus (OC43) was added at the several multiplicities of infection (moi; either 0.01, 0.02 or 0.1). Infection proceeded for 4 h, after which cells were washed with infection media and then incubated in fresh infection media plus or minus treatment. Treatments were left on for four to seven days and cells were scored for cytopathic effect daily. In experiments where virus was quantified, media was removed and stored at −80 °C for later qPCR analysis. Cell monolayers were then washed with PBS and lysed by freeze-thaw in the presence of RNAse inhibitors. Cytosolic contents were collected in RNAse-free PBS and stored at −80 °C until processing for qPCR.

Light Microscopy: Cultured cells (uninfected and Zinc treated virus-infected) were imaged using an EVOS FL Auto Imaging System (Thermo Fisher Scientific, Waltham, MA). Light images (transmitted or phase contrast) were acquired at 400X.

qPCR: Viral RNA was isolated from media and cell extracts using a Purelink viral RNA/DNA minikit (ThermoFisher Scientific, Waltham, MA). cDNA was obtained using reverse transcription with MoMuLVRT and random priming. qPCR was performed using the LUNA Universal qPCR Master Mix (NEB, Ipswich, MA). cDNA (5-fold diluted) input was at 10 % (v/v) into the qPCR reaction. Amplification and quantification were performed with an Applied Biosystems StepOnePlus real time PCR system (ThermoFisher, Waltham, MA).

3. Results and discussion

Initial experiments were carried out to test the limits for zinc concentrations on multiple cell types. These cell types included Jurkat, ARPE-19, MCF7, HCT-8, A549 and Vero cells. They were treated with zinc to determine LC50 concentrations. Cells were exposed to concentrations of Zn^{2+} ranging from 10uM to 600uM. The studies showed that zinc above a concentration of 200uM is toxic to most cell types except for Jurkat cells, where toxicity began just above 100uM. (Fig. 1).

Zn^{2+} was sometimes encapsulated with BSA to increase cholestosome yield, so Vero cells were separately exposed to zinc and zinc + BSA (with zinc as zinc chloride). Although the Zn^{2+} and zinc/BSA curve looked slightly different, the calculated LC50s were the same for each (234uM). Data from a cholestosome formulation containing zinc chloride plus BSA is also shown in Fig. 1 (see Vero (Chol-zinc chloride/BSA)). The data shows an increased LC50 afforded by encapsulating zinc (>400uM) relative to free zinc or zinc plus BSA. Similar observations were made when zinc was encapsulated as zinc sulfate (not shown).

These preliminary data indicated the maximum concentration to be tried in studies for inhibition of viral infection. Betacoronavirus OC43 (OC43) is a reasonable surrogate for general endemic infections representing several infectious respiratory viral diseases, including the common cold and influenza as well as the recent pandemic agent COVID-19 which seems to be following an evolutionary course like that which brought influenza to endemic status. OC43 and the lung carcinoma derived cell line A549, which has been considered to have an 'alveolar' phenotype [54], have been used as a model system to determine if cholestosome encapsulated Zn^{2+} could affect viral infection. In this system infection was determined by assessing the development of the virus-induced cytopathic effect (CPE) as well as assessment of the

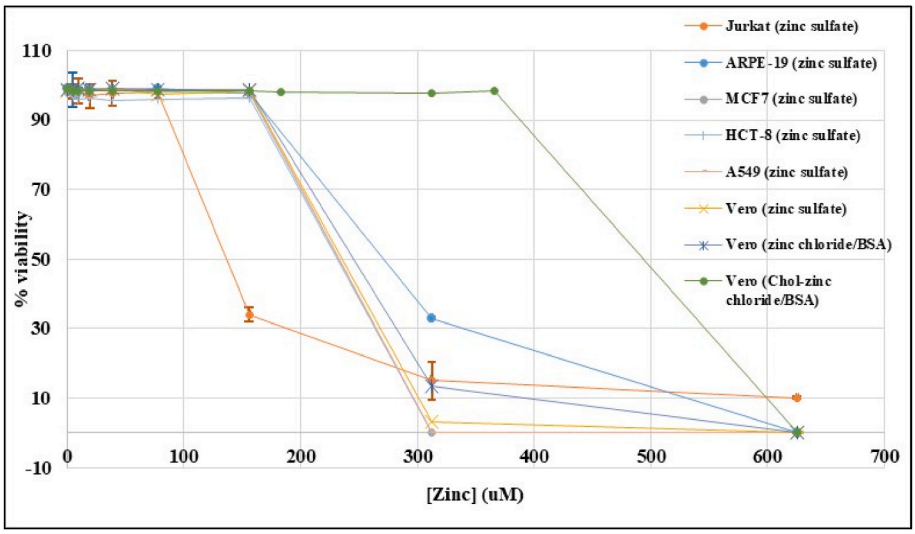

Fig. 1. Cholestosome encapsulation of zinc increases the zinc LC50. Jurkat -Vero (zinc sulfate) are zinc viability curves for various cell line targets for OC43 infection (see Key in upper right quadrant). Cell lines exposed to increasing concentrations of zinc sulfate were assayed for viability by trypan blue exclusion. The Vero (Chol-zinc chloride/BSA) curve was derived from treatment with a cholestosome-zinc chloride/BSA formulation and is shown to illustrate the increased LC50 afforded by encapsulating zinc relative to treatment with free zinc or free zinc plus BSA.

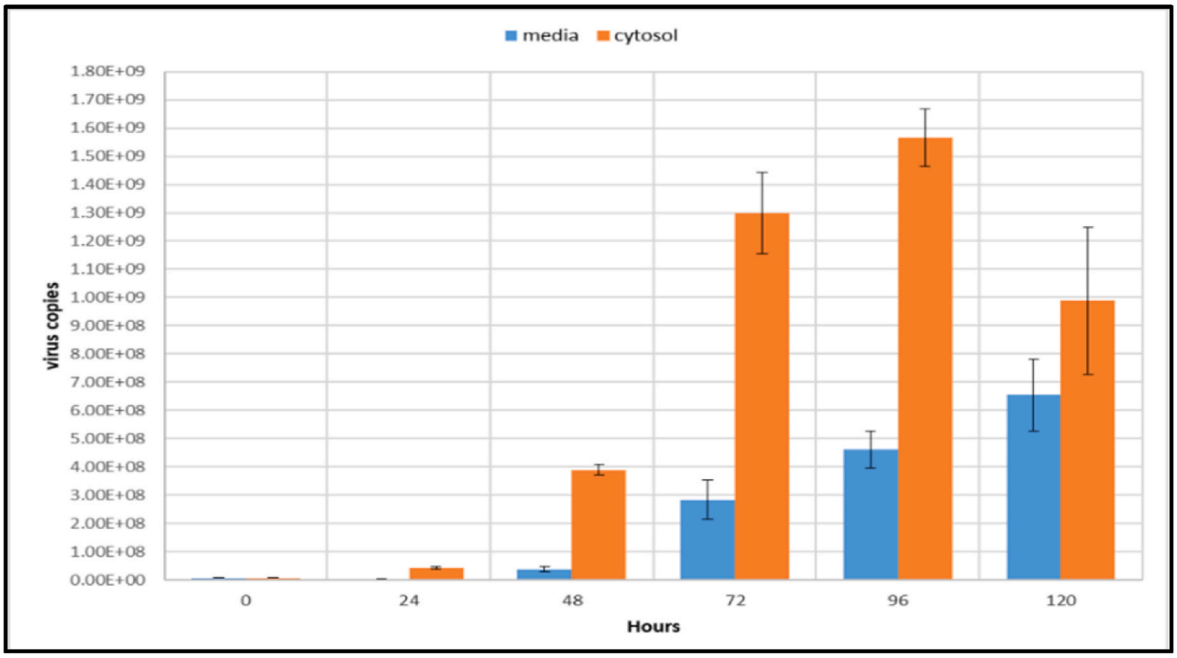

Day	0	1	2	3	4	5
% CPE						
Well: 1	0	0	0	10	80	90
2	0	0	0	15	70	90
3	0	0	0	0	60	80

Fig. 2. Time course comparison of extracellular (media) and intracellular (cell cytosol) viral load in OC43 infected A549 cells (MOI = 1) for 4 h at 33 °C, 5 % CO_2. Zero-hour virus samples were collected and stored as described in the text for later qPCR analysis. Cells were then fed fresh infection media and incubated for the indicated times. At each time point virus media was collected, cells were washed with PBS (pooled w/virus media) and monolayers were lysed by freeze thaw (−80/37 °C) in PBS containing RNAse inhibitors. Cytosolic extracts were saved at −80 °C until qPCR analysis. Top panel, Bar graphs showing the mean (± SD) of three replicate dishes for each condition. Bottom panel, table containing the results of scoring for CPE in each replicate of the cultures summarized in the graph. The percent of cells showing CPE is shown for each well. This experiment repeated with comparable results.

relative amount of viral copy number using quantitative reverse transcription-polymerase chain reaction [55]. Preliminary experiments were conducted to determine the relative agreement between the two assessment methods as well as the best time point after infection in which to assess viral load. For qRT-PCR assays, virus number was assessed separately in the cell culture media and the cytosolic fraction of the cells. Typical results from these experiments are shown in Fig. 2.

The results show an approximately one order of magnitude difference in viral numbers in the media and cytosolic pools at two days post-infection. This narrows to 4.5-fold on day three and 3.3-fold on day four post infection. By day five post-infection there is no difference in virus content in media versus cytosol. CPE scored on these day tracks inversely with the decreasing differences, being undetectable at 24 h, increasing to high levels at later times. The results suggest that at 48 h post infection, intracellular virus could be used as a surrogate measure of viral replication, allowing a simpler approach to assessing global effects on the process, independent of measurements of nascently labeled nucleic acids or polyprotein processing within the cytosolic fraction.

Fig. 3 shows the results of experiments to determine the appropriate free Zn^{2+} dose needed to inhibit propagation of OC43 in A549 cells. In these cells, free Zn^{2+} at 20uM and 50uM shows a statistically significant maximal inhibition, relative to untreated, 2uM Zn^{2+}-treated and 5uM Zn^{2+}-treated infected cells. Maximum inhibition occurred 4 days after infection (4 h at an MOI of 0.1) during which treated cells were continuously exposed to Zn^{2+} following removal of the virus (Fig. 3, compare panels E and F to panels B–D). This is shown graphically in

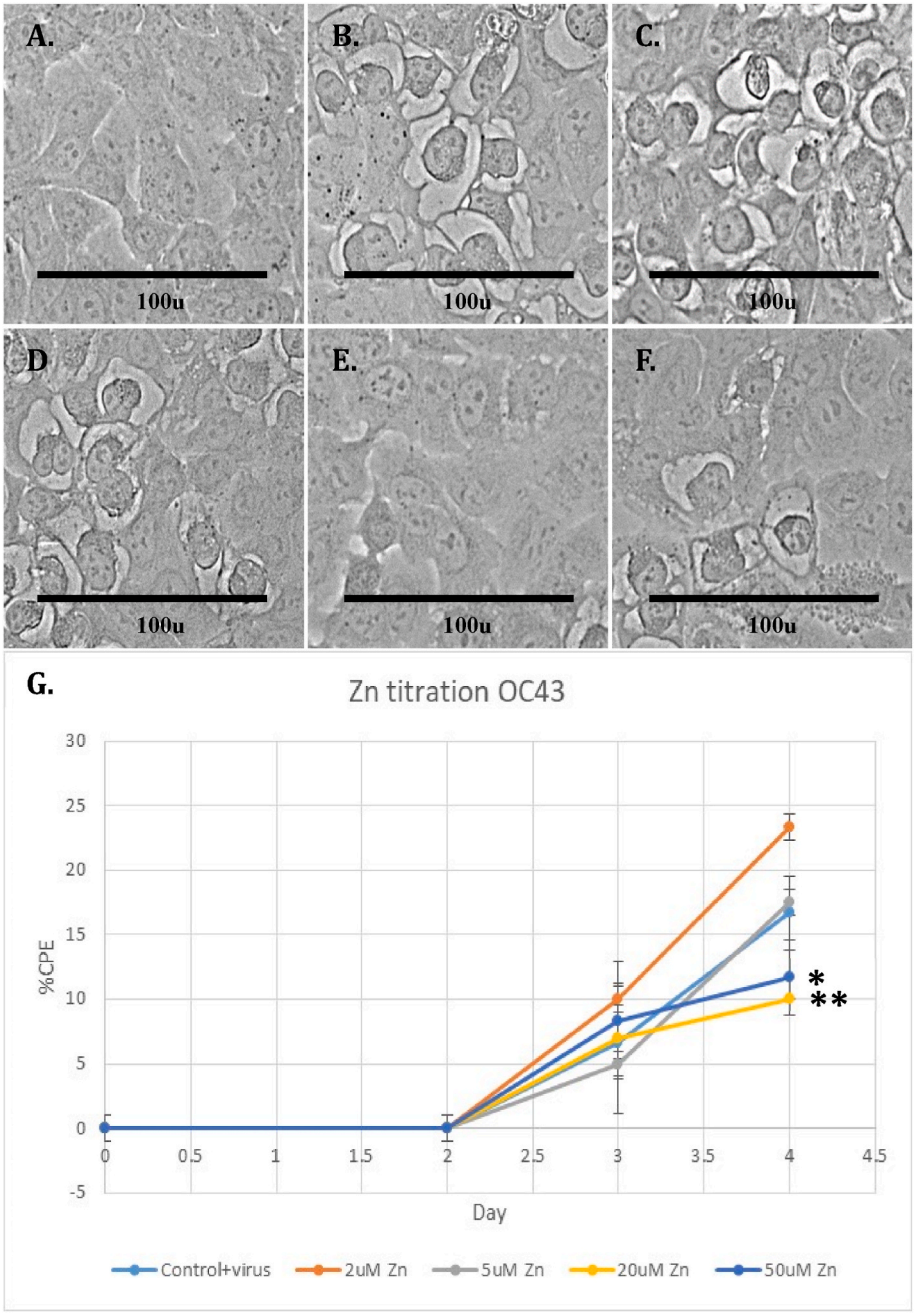

Fig. 3. Zinc treatment reduces CPE in OC43 infected A549 cells. Shown in panels A–F are phase contrast images of uninfected A549 cells (A) and A549 cells infected with OC43 and either untreated (B) or treated with zinc at 2uM, 5uM, 20uM and 50uM (C, D, E and F, respectively), size bars shown at the bottom of each panel. The graph in G shows a plot of the CPE, by day, in the cell cultures depicted in B–F. There was a reduction in CPE at this typically early time point after infection (4 days after infection at MOI = 0.09). *p = 0.05, **p < 0.05, versus untreated infected control cells; one-tailed Student's T-Test.

Fig. 3G. The overall viral load in untreated infected cells (as judged by CPE) is like that seen in untreated infected cells assayed at 3 days in Fig. 2 (MOI = 1) and is typical of the measured viral burden observed at 4 days post-infection with this MOI.

Determination of optimal Zn^{2+} fr ee concentrations informed the testing for encapsulated Zn^{2+} concentration in cholestosome vesicles. Results shown in Fig. 4 indicate a statistically significant reduction in viral production using Cholestosome-encapsulated Zn^{2+} versus free Zn^{2+}. Zinc serial dilution experiments performed in OC43 infected A549 cells were consistent with these results, also showing statistically significant reductions in viral production (2–18-fold), at multiple dilution levels, following six days of treatment relative to free zinc (not shown). Similar results were observed in repeated experiments.

4. Conclusion

To determine if use of cholestosome technology to deliver Zn^{2+} intracellularly can inhibit viral production, a series of studies with Zn^{2+} encapsulated in the cholestosome delivery system were carried out. Studies showed that a concentration of greater than 200uM extracellular free Zn^{2+} was toxic to most cells studied. Moreover, in these studies the LC50 concentration for cholestosome-encapsulated Zn^{2+} is two to four times higher than that of free Zn^{2+}. The studies conducted to assess toxicity of zinc (Fig. 1) suggest that free zinc at a concentration of greater than 150uM was required to overcome zinc homeostasis and produce cell death in cultured cells of various lineages. In people, visible and measurable effects of zinc overdose (e.g. gastrointestinal distress, copper depletion, etc.) occur after oral zinc consumption of 300 mg per day (approximately 10 %–20 % of total body content of zinc; [25,26,59]. However, if full absorption and no efflux is assumed, 300 mg would be an approximate circulating and tissue concentration of 900uM, far exceeding the toxic concentrations seen in Fig. 1. The body's exquisite regulation of zinc absorption and metabolism results in normal plasma zinc concentrations in the low micromolar range (10-20uM), free zinc at only about 0.0001 % of the total zinc pool and the bulk zinc tied up in the tissues and plasma by zinc binding proteins [25,26,60]. The tight regulation of zinc absorption and metabolism in vivo such that free zinc is a tiny fraction of total cellular zinc [25], suggests a reason that it requires such large amounts of zinc to produce sign of over consumption. It should be said that Cholestosome mediated delivery of encapsulated cargo in vitro (e.g. FITC) or in vivo (e.g. insulin) occurs steadily over time after single dose administration, in cultured cells in vitro (peaking at 24 h) and cyclically in rodents in vivo, regardless of dosing method (oral, intravenous or intraperitoneal; 39–45 and not shown). The similarity in LD50 concentrations in diverse cultured cell types suggest normal zinc regulation is not recapitulated in culture, so it is not surprising that this regulation can be overwhelmed by free zinc in cultured cells. Importantly, the present study suggests that cholestosome encapsulation can apparently allow for a more regulated delivery such that it takes 2-fold–4-fold higher concentrations of zinc for this overwhelming to occur. Further, it also suggests that cholestosome delivery of zinc can reduce zinc toxicity, not exacerbate it.

The studies show that both free and encapsulated Zn^{2+} have an impact on OC43 betacoronavirus infection but cholestosome-encapsulated Zn^{2+} decreases viral load to a greater extent than unencapsulated Zn^{2+}. Importantly, this decrease was observed in cells representing two known targets of betacoronavirus, as well as other pathogenic viruses (e.g. RSV, rotavirus; [5,48,56–58]). These results mark the first required steps towards using cholestosome encapsulated Zn^{2+} as a general antiviral treatment.

CRediT authorship contribution statement

Lawrence Mielnicki: Writing – review & editing, Writing – original draft, Investigation, Formal analysis. **Julie Hughes:** Investigation, Data curation. **Mary Irving:** Investigation, Data curation. **Mary McCourt:** Writing – review & editing, Writing – original draft, Validation, Supervision, Methodology, Investigation, Funding acquisition, Formal analysis, Data curation, Conceptualization.

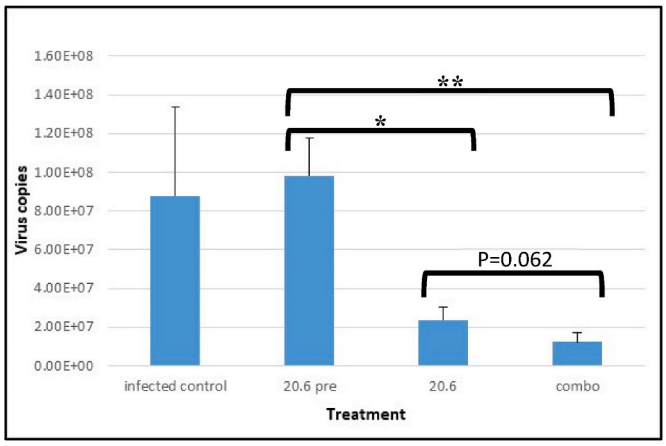

Fig. 4. Encapsulated zinc reduces viral load in OC43 infected HCT8 cells. Shown is a comparison of PCR results from zinc treatment study in OC43 infected HCT8 cells (moi = 0.02). Similar results were obtained using 3 different OC43 specific primer pairs. Sample treatment is indicated at the bottom of each panel. Virus numbers are given on the left of each panel. Infected control is virus from untreated OC43 infected cells. 20.6 pre is virus from cells treated with 20.6uM free zinc added 2h prior to and removed at the end of the 4h infection period. 20.6 is virus from cells treated with 20.6uM free zinc from the end of the 4h infection period until collection at 72h post-infection. Combo is virus from cells treated with cholestosome encapsulated zinc (at 100uM) from the end of the 4h infection period until collection at 72h post-infection. Shown are the mean ± SD of 3 replicates. Inoculant was removed at the end of the 4h infection period. *p < 0.05 versus 20.6uM zinc pretreatment; **p < 0.01 versus 20.6uM zinc pretreatment; one tailed Student's T-Test. p = 0.062 encapsulated zinc vs 20.6uM free zinc.

Declaration of competing interest

I have nothing to declare.

Acknowledgments

The authors would like to acknowledge the support of the Niagara University Chemistry Department and Academic Center for Intergrated Sciences.

Data availability

Data will be made available on request.

References

[1] R.H. Tough, P.J. McLaren, Interaction of the host and genome and their influence on HIV disease, Front. Genet. 9 (2018) 720.
[2] M.A. Myers, A.P. Smith, L.C. Lane, D.J. Moquin, R. Aogo, S. Woolard, P. Thomas, P. Vogel, A. Smith, Dynamically linking influenza virus, infection kinetics, lung injury, inflammation and disease severity, al. eLife 10 (2021) e68864, https://doi.org/10.7554/eLife.68864.
[3] K. Dhama, F. Nainu, A. Frediansyah, M.I. Yatoo, R.K. Mohapatra, S. Chakraborty, H. Zhou, M.R. Islam, S.S. Mamada, H.I. Kusuma, A.A. Rabaan, S. Alhumaid, A. A. Mutair, M. Iqhrammullah, J.A. Al-Tawfiq, M.A. Mohaini, A.J. Alsalman, H. S. Tuli, C. Chakraborty, H. Harapan, Global emerging Omicron variant of SARS-CoV-2: impacts, challenges and strategies, J Infect Public Health 16 (1) (2023 Jan) 4–14, https://doi.org/10.1016/j.jiph.2022.11.024. Epub 2022 Nov 19.
[4] E. Gusev, A. Sarapultsev, L. Solomatina, V. Chereshnev, SARS-CoV-2-Specific immune response and the pathogenesis of COVID-19, Int. J. Mol. Sci. 23 (3) (2022 Feb 2) 1716, https://doi.org/10.3390/ijms23031716.
[5] M. Cascella, M. Rajnik, A. Aleem, S.C. Dulebohn, R. Di Napoli, Features, evaluation, and treatment of coronavirus (COVID-19).2023 aug 18, in: StatPearls [Internet]. Treasure Island (FL), StatPearls Publishing, 2024 Jan. PMID: 32150360.

[6] R. Gao, W. Zu, Y. Liu, J. Li, Z. Li, Y. Wen, H. Wang, J. Yuan, L. Cheng, S. Zhang, Y. Zhang, S. Zhang, W. Liu, X. Lan, L. Liu, F. Li, Z. Zhang, Quasispecies of SARS-CoV-2 revealed by single nucleotide polymorphisms (SNPs) analysis, Virulence 12 (1) (2021 Dec) 1209–1226, https://doi.org/10.1080/21505594.2021.1911477.
[7] Shrestha, et al., Evolution of the SARS-CoV-2 omicron variants BA.1 to BA.5: implications for immune escape and transmission, Rev. Med. Virol. 32 (2022) e2381.
[8] A.M. Carabelli, et al., SARS-CoV-2 variant biology: immune escape, transmission and fitness, Nat. Rev. Microbiol. 21 (March 2023) 162–177.
[9] V. Gote, et al., A comprehensive review of mRNA vaccines, Int. J. Mol. Sci. 24 (2023) 2700, https://doi.org/10.3390/ijms24032700.
[10] R. Geraghty, et al., Broad-spectrum antiviral strategies and nucleoside analogues, Viruses 13 (2021) 667, https://doi.org/10.3390/v13040667.
[11] Simsek-Yavus, Celikyurt, An update of anti-viral treatment of COVID-19, Turk. J. Med. Sci. (2021), https://doi.org/10.3906/sag-2106-250.
[12] J.C. Jones, et al., Influenza antivirals and their role in pandemic preparedness, Antivir. Res. 210 (2023 February) 105499, https://doi.org/10.1016/j.antiviral.2022.105499.
[13] H. Khalifa, Y. Ramahi, After the hurricane: anti-COVID-19 drugs development, molecular mechanisms of action and future perspectives, Int. J. Mol. Sci. 25 (2024) 739, https://doi.org/10.3390/ijms25020739.
[14] R. Delshadi, et al., Development of nanoparticle-delivery systems for antiviral agents: a review, J. Contr. Release 331 (2021) 30–44.
[15] L. Lu, et al., Antivirals with common targets against highly pathogenic viruses, Cell 184 (2021). March 18, 2021 a Elsevier Inc.
[16] I. Sadeghian, et al., Potential of cell-penetrating peptides (CPPs) in delivery of antiviral therapeutics and vaccines, Eur. J. Pharmaceut. Sci. 169 (2022), https://doi.org/10.1016/j.ejps.2021.106094.
[17] Kaur R. et al. Restriction of SARS-CoV-2 replication by receptor transporter protein 4 (RTP4). Am Soc for Micro. July/August Volume 14 Issue 4.
[18] S.A. Read, et al., The role of zinc in antiviral immunity, Adv. Nutr. 10 (2019) 696–710, https://doi.org/10.1093/advances/nmz013.
[19] N.A. Khan, et al., Respiratory syncytial virus-induced oxidative stress leads to an increase in labile zinc pools in lung epithelial cells, Am Soc for Micro 5 (3) (2020) e00447. May/June.
[20] Kreiser, et al., Inhibition of respiratory RNA viruses by a composition of ionophoric polyphenols with metal ions, Pharmaceuticals 15 (2022) 377, https://doi.org/10.3390/ph15030377.
[21] T. Momin, A. Villasenor, A. Singh, M. Darweesh, A. Singh, M. Rajput, ZFP36 ring finger protein like 1 significantly suppresses human coronavirus OC43 replication, PeerJ 11 (2023) e14776, https://doi.org/10.7717/peerj.14776.
[22] J. Hunter, S. Arentz, J. Goldenberg, et al., Zinc for the prevention or treatment of acute viral respiratory tract infections in adults: a rapid systematic review and meta-analysis of randomized controlled trials, BMJ Open 11 (2021) e047474, https://doi.org/10.1136/bmjopen-2020-047474.
[23] Pormohammad, et al., Zinc and SARS-CoV-2: a molecular modeling study of Zn interactions with RNA-dependent RNA-polymerase and 3C-like proteinase enzymes, Int. Jour. of Molecular medicine 47 (2021) 326–334.
[24] T. Momin, A. Villasenor, A. Singh, M. Darweesh, A. Singh, M. Rajput, ZFP36 ring finger protein like 1 significantly suppresses human coronavirus OC43 replication, PeerJ 11 (2023) e14776, https://doi.org/10.7717/peerj.14776.
[25] S.A. Read, et al., The role of zinc in antiviral immunity, Adv. Nutr. 10 (2019) 696–710, 10.093/advances/nmz013.
[26] B. Chen, Cellular zinc metabolism and zinc signaling: from biological functions to diseases and therapeutic targets, Signal Transduct. Targeted Ther. 9 (2024) 6.
[27] I. Sadeghian, et al., Potential of cell-penetrating peptides (CPPs) in delivery of antiviral therapeutics and vaccines, Eur. J. Pharmaceut. Sci. 169 (2022) 106094.
[28] K. Vijay, D.N. Mishra, A.K. Sharma, B. Srivastava, Birendra, International Journal of Current Pharmaceutical Review and Research 1 (2010) 6–16.
[29] Y. Barenholz inLiposome Dermatics. Griesbach Conference.(eds Braun-Falco, O., Korting, H.C., Maibach .https://doi.org/10.1007/978-3-642-48391-2_8.
[30] A. Samad, Y. Sultana, M. Aqil, Curr. Drug Deliv. (2007) 297–305.
[31] H. Nsairat, D. Khater, U. Sayed, F. Odeh, A. Al Bawab, W. Alshaer, Heliyon 8 (5) (2022) e09394, https://doi.org/10.1016/j.heliyon.2022.e09394.
[32] A.M. Grumezescu (Ed.), Nanobiomaterials in Galenic Formulations and Cosmetics: Applications of Nanobiomaterials, 2016.
[33] S. Gelperina, K. Kisich, M.D. Iseman, L. Heifets, Am. J. Respir. Crit. Care Med. 172 (12) (2005 Dec 15) 1487–1490, https://doi.org/10.1164/rccm.200504-613PP.
[34] P.M. Finglas, Y. Rickey, R.Y. Yada, F. Toldrá, Nanotechnology in foods: science behind and future perspectives, Trends Food Sci. Technol. 40 (2) (December 2014) 125–126.
[35] Z. Qin, A. Bouteau, C. Herbst, B.Z. Igyarto, PLoS Pathog. (2022), https://doi.org/10.1371/journal.ppat.1010830.
[36] D.D. Lasic, J. Liposome Res. 9 (1) (1999) 43–52, https://doi.org/10.3109/08982109909044491.
[37] R. John, J. Monpara, S. Swaminathan, R. Kalhapure, Chemistry and art of developing lipid nanoparticles for biologics delivery: focus on development and scale-up, Pharmaceutics 16 (1) (2024 Jan 19) 131, https://doi.org/10.3390/pharmaceutics16010131.
[38] Mielnicki, L. Hughes, J., Schentag J., Irving, M., Monetti, V., MacArther, JF, Cordone, D, McCourt, M. Development of the cholestosome, a novel delivery system made exclusively from cholesteryl esters, Eur. J. Lipid Sci. Technol. Volume 126,Issue 2 2300087.
[39] M.P. McCourt, Patent: drug delivery means, Status: Issued as US 9 (119) (2015) 782, on September 1.
[40] J.J. Schentag, M.P. McCourt, L. Mielnicki, J. Hughes, Patent: cholestosome vesicles for incorporation of molecules into chylomicrons, Status: Issued as US 9 (693) (July 4, 2017) 968.
[41] M.P. McCourt, Patent: drug delivery means, Issued as US 10 (92) (2018) 516. B2 on October 9th.
[42] J.J. Schentag, M.P. McCourt, L. Mielnicki, J. Hughes, Patent: cholestosome vesicles for incorporation of molecules into chylomicrons, Status: Issued as US 10 (369) (August 6, 2019) 114.
[43] Schentag JJ, McCourt MP, Mielnicki L, Hughes J.Patent: cholestosome vesicles for incorporation of molecules into chylomicrons:Status: Issued as US 11,52,52.
[44] Schentag JJ, McCourt MP, Mielnicki L, Hughes J.Patent: cholestosome vesicles for incorporation of molecules into chylomicrons:Status: Issued as US 11,633,364.
[45] McCourt MP. Patent: drug delivery means:Status: Issued as US. 11,737,396.
[46] K. Owczarek, A. Szczepanski, A. Milewska, Z. Baster, Z. Rajfur, M. Sarna, K. Pyrc, Early events during human coronavirus OC43 entry to the cell, Sci. Rep. 8 (1) (2018 May) 7124, https://doi.org/10.1038/s41598-018-25640-0. PMID: 29740099.
[47] D.A. Sabbah, R. Hajjo, S.K. Bardaweel, H.A. Zhong, An updated review on betacoronavirus viral entry inhibitors: learning from past discoveries to advance COVID-19 drug discovery, Curr. Top. Med. Chem. 21 (7) (2021) 571–596, https://doi.org/10.2174/1568026621666210119111409.
[48] C. Savoie, R. Lippé, Optimizing human coronavirus OC43 growth and titration, PeerJ 10 (2022) e13721, https://doi.org/10.7717/peerj.13721.eCollection2022, 2022 Jul 8.
[49] G. Castillo, et al., Human air-liquid-interface organotypic airway cultures express significantly more ACE2 receptor protein and are more susceptible to HCoV-NL63 infection than monolayer cultures of primary respiratory epithelial cells, Microbiol. Spectr. 10 (4) (2022), https://doi.org/10.1128/spectrum.01639-22. July/August.
[50] S. Li, et al., Activation of the MKK3-p38-MK2-ZFP36 Axis by coronavirus infection the upregulation of AU-rich element- containing transcripts in proinflammatory responses, J. Virol. 96 (5) (March 2022) e0208621.
[51] L.M. Mielnicki, A.M. Ying, K.L. Head, H.L. Asch, B.B. Asch, Epigenetic regulation of gelsolin expression in human breast cancer cells, Exp. Cell Res. 249 (1999) 161–176.
[52] U. Schneider, H.U. Schwenk, G. Bornkamm, Characterization of EBV-genome negative "null" and "T" cell lines derived from children with acute lymphoblastic leukemia and leukemic transformed non-Hodgkin lymphoma, Int. J. Cancer 19 (5) (1977 May 15) 621–626, https://doi.org/10.1002/ijc.2910190505.
[53] K.C. Dunn, A.E. Aotaki-Keen, F.R. Putkey, L.M. Hjelmeland, ARPE-19, a human retinal pigment epithelial cell line with differentiated properties, Exp. Eye Res. 62 (2) (1996 Feb) 155–169, https://doi.org/10.1006/exer.1996.0020.
[54] J.R. Cooper, Long term culture of the A549 cancer cell line promotes multilamellar body formation and differentiation towards an alveolar type II pneumocyte phenotype, PLoS One (2016), https://doi.org/10.1371/journal.pone.0164438. October 28.
[55] J. Guo, J. Ge, Y. Guo, Recent advances in methods for the diagnosis of corona virus disease 2019, J. Clin. Lab. Anal. 36 (1) (2022 Jan) e24178, https://doi.org/10.1002/jcla.24178. Epub 2021 Dec 17.
[56] A. Antia, D.M. Alvarado, Q. Zeng, L.A. Casorla-Perez, D.L. Davis, N.M. Sonnek, M. A. Ciorba, S. Ding, SARS-CoV-2 omicron BA.1 variant infection of human colon epithelial cells, Viruses 16 (4) (2024) 634, https://doi.org/10.3390/v16040634, 2024 Apr 19.
[57] A. Agac, S.M. Kolbe, M. Ludlow, A.D.M.E. Osterhaus, R. Meineke, G. F. Rimmelzwaan, Host responses to respiratory syncytial virus infection, Viruses 15 (10) (2023) 1999, https://doi.org/10.3390/v15101999, 2023 Sep. 26.
[58] C.E. LeClair, K.A. McConnell, Rotavirus, in: StatPearls [Internet], StatPearls Publishing, Treasure Island (FL), 2023, 2024 Jan. PMID: 32644377.
[59] G.J. Fosmire, Zinc toxicity, Am. J. Clin. Nutr. 51 (2) (February 1990) 225–227.
[60] M. Rukgauer, J. Klein, J.D. Kruse-Jarres, Reference values for the trace elements copper, manganese, selenium, and zinc in the serum/plasma of children, adolescents, and adults, J. Trace Elem. Med. Biol. 11 (2) (1997) 92–98.